

Surface Studies on Industrial Aluminium Alloys

MASTER THESIS
EQUIVALENT TO 30 ECTS

Lisa Rullik
VT 2014

Supervisors:
Dr. Florian Bertram, Prof. Dr. Edvin Lundgren

Division of Synchrotron Radiation Research
Department of Physics
Faculty of Science



LUNDS
UNIVERSITET

Handed in to the examination committee on May 28th, 2014. To be presented at a public seminar in room H322 at the department of physics in Lund on June 11th, 2014 at 10am.

Copyright ©Lisa Rullik
Division of Synchrotron Radiation Research
Department of Physics
Lund University
Printed in Lund, Sweden, 2014

Making Aluminium Alloys Sweat

Aluminium based products, especially aluminium alloys, can be found in all aspects of everyday life. If you drive a car, drink from a beverage can or pass through a doorframe, aluminium alloys are used. To improve performance, lifetime and production of aluminium alloys, we need to know how they behave in different situations for example when you heat them.

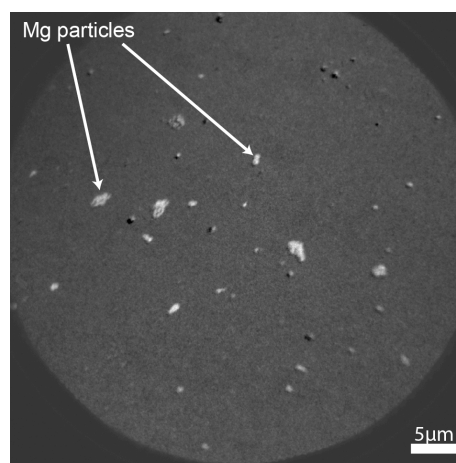
To understand how aluminium alloys react on heat treatment is important because during the production of these alloys and the joining of different work pieces, aluminium alloys are heated. Besides aluminium several other elements are present in the alloy to give it its desired properties. All of these additional elements like magnesium, silicon and iron are influenced differently by heat.

If an aluminium alloy is exposed to an oxygen rich atmosphere like air, it forms an aluminium oxide layer on its surface within seconds. For some applications this natural occurring oxide layer provides a good corrosion protection. During brazing the oxide layer on top of the alloy is disadvantageous because it disturbs the bonding between the work pieces.

For our heating experiments we used a special type of microscope called *Spectroscopic Photoemission and Low Energy Electron Microscope*, short *SPELEEM*. The SPELEEM is situated at the national Swedish synchrotron radiation facility, MAX IV Laboratory. With this microscope images with an element specific contrast can be obtained, e.g. it only shows magnesium-rich areas as bright spots as shown in the figure below. The *SPELEEM* allows taking images showing the topography of the alloys' surface, too. Further, the SPELEEM can be operated in a spectroscopy mode. Spectroscopy is the study of how matter interacts with light. Using spectroscopic techniques different chemical states of the elements in the alloy can be detected. It can be used to figure out if aluminium or aluminium oxide is present on the surface.

Using the SPELEEM in its different modes of operation we detected for both studied aluminium alloys that magnesium particles start to precipitate at the aluminium alloy surface when you heat it to 400°C.

For the aluminium alloy that is used in brazing applications we found that the aluminium oxide layer decomposes at 490°C, but that small islands of the aluminium oxide film still remain on the surface.



Supervisors: **Dr. Florian Bertram, Prof. Dr. Edvin Lundgren**

Master thesis corresponding to 30 ECTS in physics, 2014

Department of Physics, Division of Synchrotron Radiation Research, Lund University

Abstract

Aluminium alloys are used in a wide range of applications due to their high tensile strength concomitant with low density. Additionally, aluminium alloys form a naturally occurring and passivating oxide layer, which leads to high corrosion and weathering resistance. In industrial manufacturing, aluminium alloys acquire their desired properties through specially designed heating processes. A common method to join aluminium work pieces together is brazing. The work pieces designed for brazing applications are coated with an aluminium alloy, which has a lower melting point as the base material. During brazing the top alloy is molten and the covering oxide layer needs to be broken up to achieve a strong and durable connection between the work pieces.

This thesis present how temperature treatment affects the surface layer of two different aluminium alloys. The processes taking place during heat treatment were studied by a combination of microscopy and spectroscopy techniques. Both alloys were heated in an UHV chamber and characterized after subsequent heating by using different operational modes of the SPELEEM (Spectroscopic PhotoEmission and Low Energy Electron Microscope). The SPELEEM is situated at beamline I311 at the MAX II storage ring at the national Swedish synchrotron radiation facility, MAX IV Laboratory. The operation modes of the SPELEEM that were used for this study are MEM (Mirror Electron Microscopy), XPEEM (X-ray PhotoEmission Electron Microscopy) and XPS (X-ray Photoelectron Spectroscopy). In addition, the samples were examined by SEM (Scanning Electron Microscopy) before and after the heat treatment.

Using the above described combination of different surface science techniques, the changes occurring upon heat treatment at the aluminium-magnesium-silicon alloy 6063 surface were studied at room temperature and after heating to 300°C and 400°C. The aluminium alloy used in brazing applications was studied at higher temperatures up to 500°C to follow the decomposition of the aluminium oxide layer. Using the previously mentioned techniques allows to follow the diffusion, reactions and sublimation of the different elements.

Acknowledgements

First of all I would like to thank my supervisors Florian Bertram and Edvin Lundgren. I have been enjoying working together with you and Jonas Evertsson.

Further, I would like to thank Alexei Zakharov and Yuran Niu for their work with the SPELEEM.

I would like to thank Simon Tågerud for recording the SEM images.

The aluminium samples were provided by Sapa Technology and Gränges Technology. Thank you Jan-Olov Nilsson, Linda Ahl and Torkel Stenqvist for answering my questions about the alloys.

My office girls, I would like to thank you for always sharing a laugh with me even if the joke wasn't funny. In my world aluminium related jokes are simply hilarious!

The lunch room community is acknowledged for the most random discussions and a great deal of Swenglish.

Special thanks goes to Anneli Nilsson-Ahlm and Patrik VVirgin, known as Padde.

I would also like to express my gratitude towards Konungariket Sverige and its tax payers for providing tuition free higher education for Europeans.

Last but not least I would like to thank Karl Niclas Viktor Johansson for making Lund feel like home.

... and finally I would like to say to you all:
Tack så mycket! Thanks a lot! Dankeschön!

Abbreviations, Constants and Symbols

c	speed of light
CCD	charge-coupled device
CL	core level
e	elementary charge
E	energy
E_B	binding energy
E_f	energy of final state
E_F	Fermi energy
E_i	energy of initial state
E_I	ionization potential
E_k	kinetic energy
E_{vac}	vacuum energy level
ESCA	electron spectroscopy for chemical analysis
h	Planck's constant
$I(x, y)$	intensity
m_0	rest mass
MEM	mirror electron microscopy
P_s	radiated power
PE	photoelectron
R	bending radius
SEM	scanning electron microscopy or microscope
SPELEEM	spectroscopic photoemission and low-energy electron microscope
T_m	melting temperature
UHV	ultra-high vacuum
UV	ultra-violet
VB	valence band
wt.%	weight percent
XP	x-ray photoelectron
XPEEM	x-ray photoemission electron microscopy
XPS	x-ray photoelectron spectroscopy
ϵ	permittivity of free space
ν	frequency
ρ	density
σ	tensile strength
σ_s	specific strength
Φ	work function

Contents

1	Introduction	1
1.1	Aluminium Alloys	1
1.2	Surface Science	3
2	Experimental Set-up and Methods	4
2.1	Synchrotron Radiation	4
2.2	Beamline I311	5
2.3	Spectroscopic Photoemission and Low Energy Electron Microscope	6
2.3.1	X-ray Photoelectron Spectroscopy	7
2.3.2	X-ray Photoemission Electron Microscopy	8
2.3.3	Mirror Electron Microscopy	10
2.4	Scanning Electron Microscopy	11
3	Aluminum-Magnesium-Silicon Alloy 6063	12
3.1	Experimental Procedure	13
3.2	Results and Discussion	14
3.2.1	Pristine Surface	14
3.2.2	XPS and XPEEM	15
3.2.3	Surface after Heat Treatment	19
3.2.4	Summary	19
4	Industrial Alloy for Brazing Applications	21
4.1	Experimental Procedure	22
4.2	Results	22
4.2.1	Pristine Surface	22
4.2.2	XPS and XPEEM	23
4.2.3	Surface after Heat Treatment	27
4.2.4	Summary	28
5	Comparison and Discussion	29
6	Conclusion and Outlook	31
7	Self-reflection	33
	Bibliography	34

1 Introduction

Materials and their industrial processing can only be designed and optimized in an efficient way if the structure-property relationship is understood to a sufficient extent. Materials containing several constituents, e.g. alloys, obtain their macroscopic properties through the interactions of their individual components on an atomic scale.

The manufacturing process of materials usually consists of several processing steps. During each process the material is exposed to a certain set of conditions. These changing environments influence the interaction between the individual components and their distribution within the material, which will lead to altered properties of the materials itself. Therefore, it is desirable to foster the understanding of atomic interactions in materials and determine how they are influenced by conditions that are characteristic to their manufacturing. The goal of this thesis project is to contribute to the described issue with regard to aluminium alloys and their manufacturing processes.

1.1 Aluminium Alloys

Aluminium alloys are used in a wide range of items because of their characteristic properties. They can be found nearly anywhere from lightweight pieces in space shuttles, aeroplanes, cars or as construction materials in skyscrapers down to ladders and beverage cans.

An exceptional property of aluminium alloys is their tensile strength, which is comparable to that of steel at low temperatures. The high tensile strength is concomitant with low density gives aluminium alloys a high specific strength. A high specific strength is desirable for materials used in transportation because the light weight can reduce energy consumption. This reduction goes together with reduced mileage and exhaust emission, which itself is preferable from an environmental perspective [1].

Additionally, aluminium products can be recycled several times without losing their high quality and that by only consuming a small fraction of the energy used to extract primary aluminium. Hence, the recycling of aluminium is preferable from an economic perspective and environmentally friendly. An in depth discussion of this aspect can be found here [2].

Further remarkable characteristics of aluminium alloys are the high thermal and electric conductivity, good machinability, castability and workability. On top of that, aluminium alloys form a passivating native oxide layer on the surface upon exposure to air or an oxidizing atmosphere, which leads to high corrosion-, weathering- and wear resistance [3,4].

1 Introduction

Aluminium alloys undergo several manufacturing processes, which are necessary to create their characteristic properties. This thesis is part of a project that focuses on studying the influence on aluminium alloys through two kinds of fabrication steps: thermal treatment and anodizing of aluminium alloys. However, the work presented here is focusing on the effects of thermal treatment of industrial aluminium alloys.

During the production of an alloy different ways of improving the properties of the material are available, e.g. strengthening mechanisms like work hardening, solute hardening, precipitation hardening and grain size hardening. In the last three mentioned strengthening mechanisms the temperature plays an important role.

In solute hardening dissolved alloying elements replace aluminium atoms in the lattice to create local distortions in it. The created strain in the lattice increases the energy barrier a dislocation needs to overcome to pass. To strengthen an alloy in this way, the composition and the solid solubility of the alloying elements are important. Generally, the solubility increases with increasing temperature.

In precipitation hardening a supersaturated solid solution is created by heating the alloy above the solvus temperature but staying below the liquidus temperature and then rapidly cooling, quenching, it. The supersaturated solid solution decomposes to get into equilibrium again and thereby forming fine precipitates. This decomposition can be increased by heating the alloy. This is usually referred to as artificial ageing. The formation of precipitates at room temperature is called ageing only. The strengthening effect occurs for coherent precipitates by the formation a strain field around the precipitate, which stops the movement of dislocations [5, 6].

Further, the grain size, which affects the creep and fatigue resistance, is influenced by the cooling rate and temperature, meaning that fast cooling leads to smaller grains [7]. Another application where the temperature is important in the processing of aluminium alloys is brazing. Brazing sheets can be used to form the final aluminium product, e.g. car frames and heat exchangers, by brazing single pieces together. These brazing sheets consist of a core material with a braze cladding on top, which itself is covered by a native oxide film. To be able to braze different compounds together effectively, the thickness of the native oxide layer and it's composition in the surface layer must be well known. This is because the native oxide layer needs to be broken without melting the core alloy but allowing the brazing alloys to flow sufficiently between the two objects to be joined [8, 9]. Further, another important processing step should be mentioned here: the growth of a thick protective oxide layer. It is realized through the oxidation of aluminium to aluminium(III) oxide. Oxidizing aluminium electrochemically is referred to as anodizing [10]. During anodizing an external current is applied in the presence of an electrolyte to the aluminium piece, which serves as the anode, hence the name. The growth of the protective oxide layer by anodizing is strongly dependent on what kind of surface it is grown on. Therefore, anodizing properties are another reason to study the effects of heat treatment on aluminium alloys.

1.2 Surface Science

Even though the surface only contributes to a small percentage of the volume of a material, it is of major importance for its performance. The surface layer of a material experiences various kind of conditions that can lead to its failure. Several failure modes, e.g. wear, thermal shock, and corrosion, are directly related to the material's surface. Additionally, the properties of the surface greatly influence how good a material can be processed further, e.g. brazing, anodizing or dyeing. Hence, it is necessary to not only study the behaviour of the whole material but specifically investigate the surface.

Surface science provides a wide range of techniques that can be applied to study how aluminium alloys are affected by heating. Here, a combination of spectroscopic and microscopic methods was used, namely x-ray photoelectron spectroscopy (XPS), x-ray photoemission electron microscopy (XPEEM) and mirror electron microscopy (MEM). The mentioned techniques were applied through a combined instrument, the Spectroscopic Photoemission and Low Energy Electron Microscope (SPELEEM), which is situated at beamline I311 at the MAX II storage ring at the national Swedish synchrotron radiation facility, MAX IV Laboratory. The SPELEEM is a powerful tool for surface science because not only changes in the chemical state of the different alloying elements can be detected but also where these changes occur by adding the information from microscopy techniques.

Additionally, optical microscopy and scanning electron microscopy (SEM) were utilized to obtain topological information before and after the heat treatment, which took place within the SPELEEM instrument. The main focus of this experimental work lies however with the SPELEEM.

Topological changes can be detected through the microscopy techniques like MEM and SEM. To get a more detailed picture about what is happening during thermal treatment of the aluminium alloy, changes in the chemical state of the single alloying elements, like oxidation and reduction, are of interest, too. These changes can be studied by techniques based on photoelectron emission, here XPS and XPEEM.

The surface sensitivity of these techniques is based on the strong interaction of electrons with matter. Electrons can only travel a certain distance without losing energy depending on their initial energy and the material they travel through. The inelastic mean free path refers to this average distance and it is in the range of ångströms depending on their kinetic energy.

Further, XPS allows, because of its surface sensitivity to study elements at different probing depths by measuring at different photon energies. This can be used to obtain insights about the kinetics during heat treatment.

2 Experimental Set-up and Methods

To study how aluminium alloy surfaces are affected by annealing different surface science techniques, namely XPS, XPEEM, MEM and SEM, were used. Topographic information about the aluminium alloy surface were obtained by MEM and SEM. XPEEM images the spatial distribution of an element in one specific chemical state. Using XP spectra the chemical states present in the sample can be identified.

The previously mentioned techniques can be separated into two groups. On the one hand there are MEM and SEM, where electrons interact with the sample's surface and on the other hand x-rays are used in XPS and XPEEM to create photoelectrons (PE), which then contain the information about the sample's surface. The x-rays used in the experiments presented here, were generated through an undulator in a storage ring. Previously, sources that created x-rays through bending magnets were parasitically implemented at synchrotrons, therefore, the light produced like that is still referred to as synchrotron radiation, even though nowadays dedicated storage rings are used to create synchrotron radiation.

2.1 Synchrotron Radiation

From classical electrodynamics it is known that if charged particles are accelerated they emit energy in form of electromagnetic waves. However, the total radiated power of non-relativistic particles is very small and scales only with the square of the change of the charged particles momentum, as described by Larmor [11].

In accelerators, which are used to produce synchrotron radiation, relativistic particles, means particles with velocities close to that of light, are used. Thus, they need to be described by relativistic electrodynamics. This is done by applying a Lorentz transformation to time and momentum. By further considering, that the charged particles are accelerated on a circular path, as in a bending magnet, the following expression can be derived, as done by Liénard [12], where c is speed of light, ϵ_0 the permittivity of free space and R the bending radius of the particles orbit

$$P_s = \frac{e^2 c}{6\pi\epsilon_0} \frac{1}{(m_0 c^2)^4} \frac{E^4}{R^2} \quad (2.1)$$

In equation 2.1 the radiated power, P_s , for particles with the elementary charge, e is proportional to the fourth power of the particle energy, E , and inversely proportional to the fourth power of the rest mass, m_0 . Thus, only particles with a low rest mass, usually electrons, at relativistic velocities can be used to produce synchrotron radiation.

By combining several short bending magnets with alternating polarity into an undulator

or wiggler, the electrons are forced onto an sinusoidal path, which allows the production of more intense and collimated radiation. Today dedicated storage rings are used instead of synchrotrons because they operate at constant energy and thus, provide a more stable beam. Figure 2.1 illustrates simplified how synchrotron radiation can be produced by sending relativistic electrons through an insertion device.



Figure 2.1: Simplified schematic of a synchrotron radiation source. Relativistic electrons circulate in the storage ring. By passing through the alternating magnetic field of the insertion device, here an undulator or wiggler, electrons are forced onto an oscillating path, which leads to the emission of synchrotron radiation.

All in all the advantages of using synchrotron radiation sources are high intensity, good tunability with respect to the wavelength, low divergence and a small beam size. A more complete description can be found here [13, 14].

2.2 Beamline I311

The main part of the experimental work was performed at the microscopy endstation of beamline I311. Beamline I311 is a soft x-ray undulator beamline with two endstations positioned at the 1.5 GeV MAX II electron storage ring at the national Swedish synchrotron radiation facility, MAX IV Laboratory, in Lund.

At the microscopy endstation of beamline I311 x-rays in the energy range from 43 eV to 650 eV can be used for experiments; at the spectroscopy endstation x-rays with an energy up to ~ 1500 eV are available. The energy resolution of the x-rays varies from 5×10^3 to 2×10^4 . The photon flux changes with photon energy and harmonic chosen as shown in figure 2.2. It is important to know this feature of the beamline to be able to normalize the measured data during the analysis, otherwise the comparison of different spectra is impossible.

A full description of beamline I311 and its properties can be found here [15].

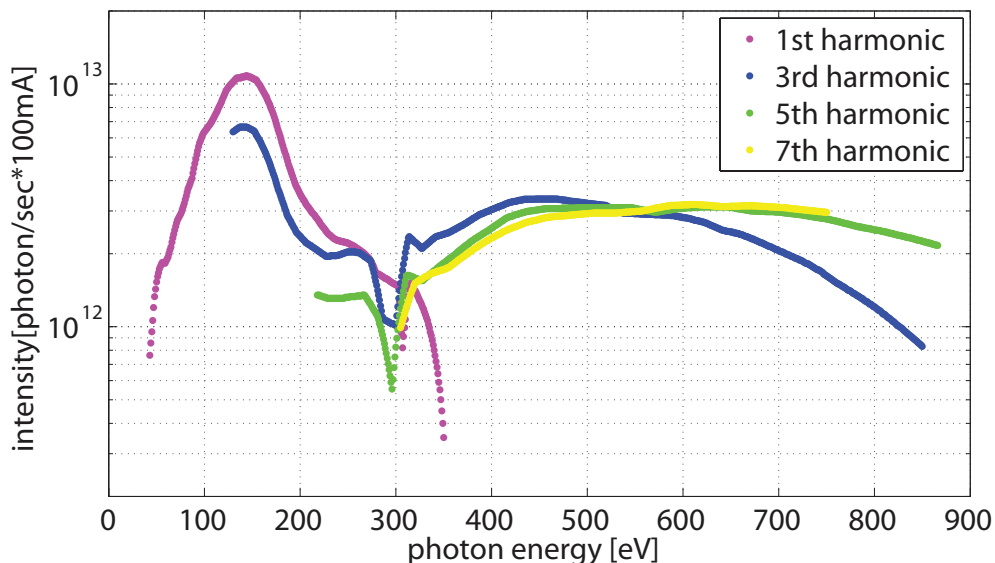


Figure 2.2: Plot photon energy vs. photon intensity for different harmonics at beamline I311. Knowing how the intensity varies with energy allows to normalize the measured spectra.

2.3 Spectroscopic Photoemission and Low Energy Electron Microscope

The here presented XPS, XPEEM and MEM measurements took place at the Elmitec SPELEEM III [16], which is situated at the microscopy endstation of beamline I311. In addition to the already mentioned modes of operation, the SPELEEM can be used for low energy electron microscopy (LEEM), low energy electron diffraction (LEED) and UV-photoemission electron microscopy (UV-PEEM). Combining all these techniques in one instrument, makes the SPELEEM a powerful tool for surface science. The different modes of the SPELEEM used for this project will be introduced later in this section.

A schematic drawing of the set-up of the SPELEEM is shown in figure 2.3. There are three different sources to illuminate the sample: a mercury UV-lamp (~ 4.8 eV), a tunable synchrotron light source (43 eV - 650 eV) and a lanthanum hexaboride cathode (-20 keV) serving as an electron gun. The electrons can be decelerated by an electric field, so that their energy can be $-20 \text{ keV} \pm \text{SV}$ (starting voltage) when they reach the sample's surface.

The beam of electrons from the electron gun is focused in the illumination column and deflected by 60° towards the sample in the magnetic beam separator. After the sample interacted either with the electrons or photons, the outgoing electrons are deflected by the beam separator again. The electrons are accelerated again and pass through another imaging column and the hemispherical electron energy analyser. Finally, the electrons

2 Experimental Set-up and Methods

are projected onto a micro channel plate (MCP) with a phosphorous screen. For creating XP spectra the dispersive plane of the hemispherical energy analyser is imaged onto the screen. By adjusting the focusing strength of the different lenses in the imaging columns, the operator can choose between projecting the gaussian image plane, which is corresponding to a real space image as used in MEM and LEEM, or the back focal plane of the objective lens, which shows the diffraction pattern as needed for LEED experiments.

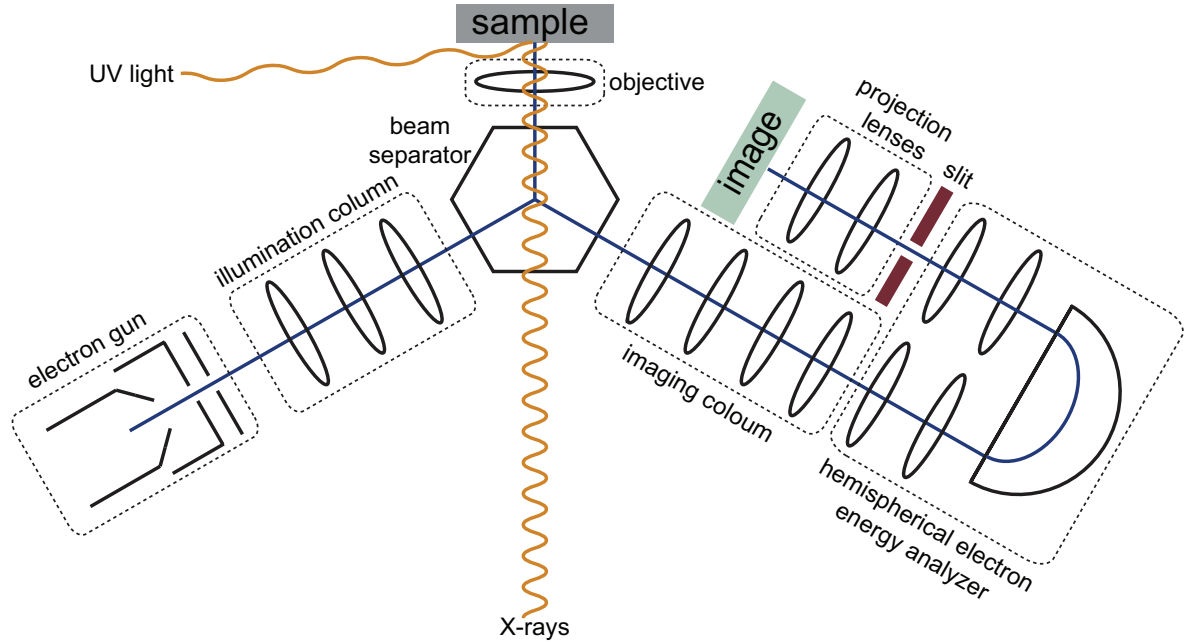


Figure 2.3: Schematic drawing of the SPELEEM instrument. The orange lines show the path of the photons; the blue line indicates the electron's path; the ellipsoids represent electron lenses. The sample can be excited by three different sources: x-rays from the synchrotron source, an electron gun (LaB₆ cathode) and a UV-lamp (Hg, ~ 4.8 eV). The resulting images are recorded by a CCD camera.

2.3.1 X-ray Photoelectron Spectroscopy

Choosing to illuminate the sample with x-rays from the synchrotron allows to take XP spectra with the SPELEEM. The processes taking place during an XPS experiment can be explained by the simplified three step model [17]. A more rigorous treatment of the theoretical background on photoionization can be found in [18].

In the first step a photon with an energy of $h\nu$, where h is Planck's constant and ν is the frequency of the radiation, impinges the surface and excites an electron with the initial energy E_i . After the excitation the electron is transported to the surface and has a final state energy of E_f . Finally, the electron has to overcome the vacuum barrier

2 Experimental Set-up and Methods

and becomes a free electron, which has a kinetic energy of E_k . Invoking the law of conservation of energy, the following equation can be deduced

$$E_i + h\nu = E_f + E_k \quad (2.2)$$

By considering that the difference between the initial energy E_i and the final energy E_f is equal to the ionization potential E_I , which itself is equal to the sum of binding energy E_B and work function Φ of the sample, we can rearrange equation 2.2 to arrive at

$$E_k = h\nu - E_B - \Phi \quad (2.3)$$

From equation 2.3 one can see that by detecting the kinetic energy, E_k , it is possible to extract the binding energy, E_B , if a monochromatic light source with a known photon energy, $h\nu$, is used and the work function, Φ , is known.

The theoretical concept behind XPS is the photoelectric effect, which originally says that metals emit electrons when they are irradiated by light. This was discovered by H. Hertz [19] in 1887. A. Einstein [20] explained this phenomenon in 1905 and later he was awarded the Nobel Prize in physics in 1921 "for his services to Theoretical Physics, and especially for his discovery of the law of the photoelectric effect" [21].

K. Siegbahn discovered that the core level binding energy of an electron is influenced by its chemical surroundings and he coined the term electron spectroscopy for chemical analysis (ESCA) [22]. In 1981 K. Siegbahn received the Nobel Prize in physics "for his contribution to the development of high-resolution electron spectroscopy" [23]. Since the chemical surrounding of the atom, whose core level electron was excited, can be deduced from an XP spectrum, XPS measurements give information on electronic and chemical state of the atom.

To detect these differences in the chemical environment, XP spectra as shown in figure 2.4 are collected and analysed according to equation 2.3. Changes in the chemical environment result in shifts of the peak positions in the spectrum.

Concerning aluminium alloys: XPS can be utilized to identify the chemical state of the alloying elements and remainder, here aluminium.

2.3.2 X-ray Photoemission Electron Microscopy

In XPEEM the sample is illuminated by a relatively wide beam of x-rays and the whole surface area is imaged simultaneously similar to a conventional optical microscope. To obtain high-resolution and surface sensitivity, the PEs emitted through the photoexcitation are used to create the image. Three different kinds of PEs can be used for imaging: core-level PEs, valence band PEs and secondary PEs. The photoexcitation process takes place as described previously for XPS in 2.3.1.

To obtain XPEEM images instead of XP spectra, a slit is inserted behind the hemispherical energy analyser in the SPELEEM, see figure 2.3. By using the slit a certain energy from the dispersive plane can be selected for imaging. By adjusting the strength of the lenses the photoelectrons can be refocused and a real space XPEEM image of the sample is projected on the screen.

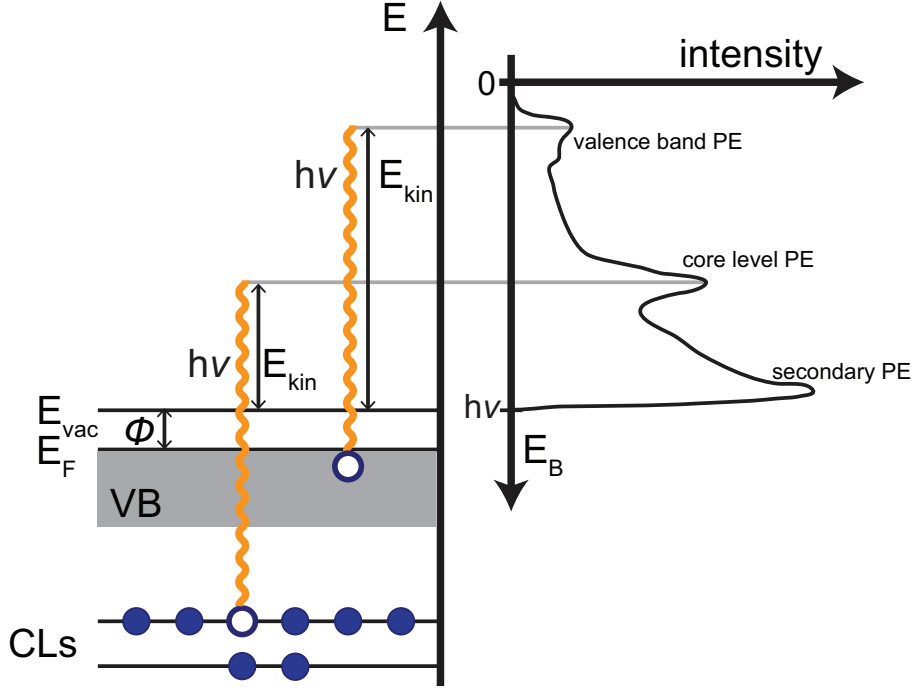


Figure 2.4: Schematic representation of the PE emission process for a typical XPS experiment and its correspondent XP spectrum. A system is excited by an incoming photon with the energy $h\nu$. After the excitation an electron is transported to the surface and overcomes the vacuum barrier. The resulting ejected electron has a kinetic energy of E_{kin} . PEs give rise to peaks in the XP spectrum with a corresponding intensity. (Energy diagram not drawn in scale.)

The contrast in the image is defined as the variation of intensity $I(x, y)$ over the image. If $I(x, y) = const$, a uniform image with no distinct features is created. To obtain and interpret XPEEM images the underlying contrast mechanisms and their physical meaning need to be considered. The following properties among others can give rise to an image contrast: work function, chemical composition, surface orientation, electronic structure, local electrostatic fields (microfields) due to topographical defects, areas of altered conductivity, partial charging and magnetic domains. Each of these properties contributes stronger or weaker to the overall contrast depending on which mode of operation is chosen, e.g. the contribution of work function contrast is high when using low excitation energies but very weak at high excitation energies [24].

In this work, mainly high photon energies were used to eject electrons from core levels. Therefore, the contrast is mainly due to electronic structure and the chemical environment of the selected species. Hence, images, taken at an excitation energy specific for a certain atom or ion, show areas with a high concentration of the chosen species as bright spots [25]. This allows to directly identify spatial distribution of a specific atom or ion.

2 Experimental Set-up and Methods

A lateral resolution of around 20 to 30 nm can be achieved in XPEEM images. Additionally, the topography of the surface influences the contrast. Features, e.g. scratches and particles on the surface, alter the potential and lead to deflection, focusing or defocusing of the photoelectrons. How this microfields affect the images is also depending on other experimental parameters, e.g. accelerating voltages [26]. Examples of how the topography of a sample influences the contrast is shown in figure 2.5. A summary of the historic development of XPEEM over the past 80 years can be found here [27].

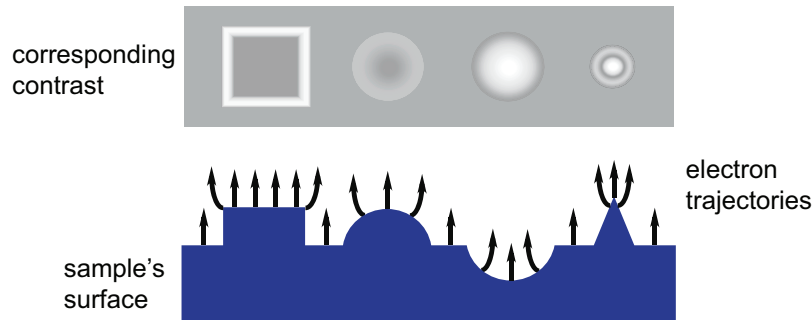


Figure 2.5: Illustrative examples of how the topography of the samples surface influences the contrast in the image. Features on the surface create microfields that cause deviation in the photoelectrons path leading to an altered contrast in the resulting XPEEM/MEM image. (adjusted, taken from [24, 26])

2.3.3 Mirror Electron Microscopy

In MEM electrons are reflected by an equipotential surface several nanometers above the real surface [28]. Electrons are accelerated towards the sample with very low kinetic energies. Before the electrons can penetrate the sample, they are reaccelerated back from the sample towards the cathode, which is the objective lens in the SPELEEM. The contrast in the resulting image is created through microfields introduced by features on the surface. As previously mentioned for XPEEM in 2.3.2 and illustrated in 2.5, microfields disturb the trajectory of the electrons on the way towards and back from the equipotential surface and thus create the contrast in the MEM image. In comparison to XPEEM, where the microfields just contributed as a disturbance in the chemical contrast, MEM uses mainly the local electric fields on the sample's surface as contrast mechanism. Additionally to the topography of the surface and its work function, other properties can have minor contributions, too [29].

2.4 Scanning Electron Microscopy

Since the SEM measurements only amount to a small part of the presented work, only a short overview to this technique will be given in the following.

In contrast to MEM, electrons in SEM have a high kinetic energy and the focused electron beam is raster scanned over the surface to create an image. Through the interaction between the electrons and the sample a range of primary and secondary signals, e.g. backscattered electrons, are created containing the information about the sample's surface. By selecting different modes of operation the contrast in the image can be altered to show the desired features [30].

The SEM images presented in this work were taken with a Hitachi SU8010. For obtaining images showing the topography of the sample's surface, secondary electrons were used. The resolution for the images depends on the kinetic energy of the electrons and is about 1.3 nm at 1 kV and about 1.0 nm at 15 kV.

3 Aluminum-Magnesium-Silicon Alloy 6063

Aluminium alloys with magnesium and silicon as their main alloying elements, are grouped together in the aluminium alloy series 6000. Alloys of the 6000 series are used in a wide range of applications due to their composition because magnesium silicide can form during quenching or artificial ageing, which improves the maximum attainable strength values [3].

The different standardized compositions of these alloys can be identified by their last three digits. In this case the aluminium-magnesium-silicon alloy 6063, which is one of the most popular alloys among the 6000 series, was studied. The chemical composition of this alloy is shown in table 3.1. A complete list of aluminium alloy standards can be found on the homepage of 'The Aluminium Association' [31].

Common applications of the aluminium alloy 6063 include heat exchangers, heat sinks, electrical components and conduits, construction products, frames and railings. Characteristic properties of aluminium alloy 6063 are very good corrosion resistance and weldability [3].

element	wt.%
Al	remainder
Mg	0.45-0.90
Si	0.20-0.60
Fe	0.35 max
Ti	0.10 max
Cr	0.10 max
Mn	0.10 max
Cu	0.10 max
Ti	0.10 max

Table 3.1: Table summarizing the chemical composition by weight percentage of the aluminium-magnesium-silicon alloy 6063 [32].

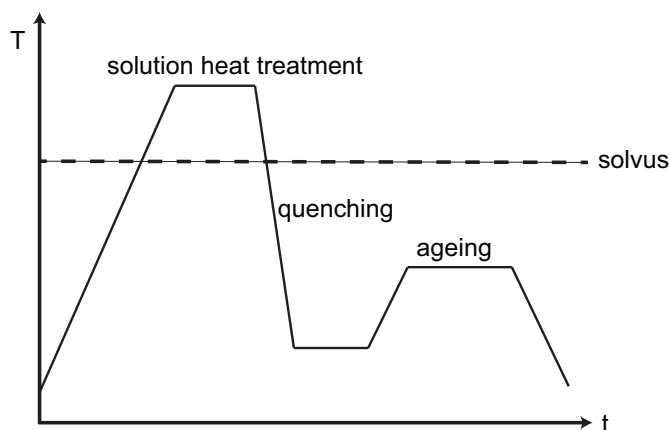


Figure 3.1: Graphic showing the heat treatment during the production of the aluminium-magnesium-silicon alloy 6063 including solution heat treatment, quenching and ageing.

The four digit-number for identifying the composition is followed by a temper designation, giving information about how the alloy was treated during the production process. The temper designation T6 which refers to aluminium alloys that have been solution heat treated and then artificially aged as the alloy that was studied here [32].

A schematic about the general layout of heat treatment during the production of an aluminium alloy 6063-T6 is found in figure 3.1. Solution heat treatment takes place at a temperature above the solvus line, which separates an area of one solid solution from an area of a mixture of solid solutions in a phase diagram. Heating the alloy above the solvus temperature, allows the formation of a solid solution containing all the alloying elements, which later should contribute to the hardening effect. During the solution heat treatment the alloying elements become uniform distributed, too. Therefore, it can be also referred to as homogenizing. The cooling rate at which the alloy is quenched needs to be high enough to keep the alloying elements dissolved in the aluminium matrix and to prevent formation of other unwanted phases. Artificial ageing, also known as precipitation hardening, is then used as a strengthening process by allowing coherent phases to precipitate [33].

3.1 Experimental Procedure

The sample preparation for the experiments on the aluminium alloy 6063-T6 is illustrated in figure 3.2. Small discs were cut out of the raw aluminium profile and polished afterwards. Before mounting the disc on the sample holder of the SPELEEM, it was cleaned with ethanol in an ultrasonic bath. The aluminium alloy sample inside the sample holder was then mounted in the UHV (10^{-10} mbar) chamber of the SPELEEM.

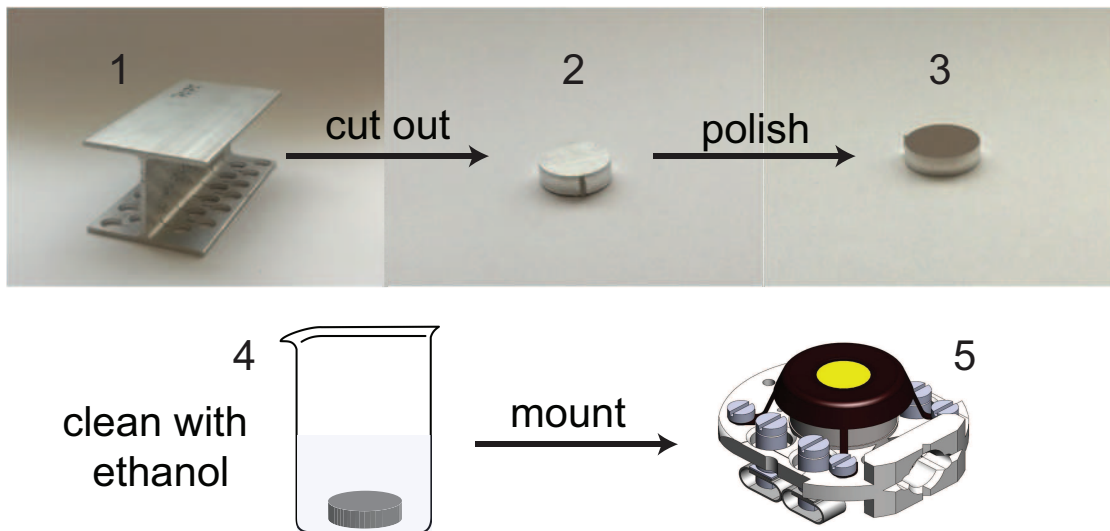


Figure 3.2: Figure showing the sample preparation. From the raw product (1) small discs (2) are cut out and polished. The polished sample (3) is cleaned with ethanol (4) in an ultrasonic bath and the mounted onto the sample holder (5).

Measurements in XPS, XPEEM and MEM mode were performed at room temperature and after subsequently heating to 300°C and 400°C. The samples were heated for

15 minutes and then cooled down at a rate of $10^{\circ}\text{C}/\text{min}$ to about 100°C for data acquisition. The cooling before the measurement is necessary to prevent arcing. The temperature was measured with the thermocouple installed at the sample holder and a Minolta/LAND Cyclops 41 Pyrometer with a fixed emissivity of 0.4, which corresponds to oxidized aluminium. Both ways of measuring the temperature are not very accurate. The thermocouple is only measuring the temperature next to the sample and not directly the sample's temperature. The pyrometer is sensitive to the emissivity but that changes with changing composition. The here shown temperatures correspond to the values obtained by the pyrometer.

Additionally, SEM images were recorded of the sample before and after the experiment at the SPELEEM with the Hitachi SU8010 SEM. The topography of the sample's surface was imaged using secondary electrons.

3.2 Results and Discussion

3.2.1 Pristine Surface

The surface topography of the aluminium alloy at room temperature is shown in the MEM image in figure 3.3. The straight lines correspond to scratches on the sample that were caused during the manufacturing process. As described previously, the cooling rate during quenching affects the grain size. Grains in this alloy usually have a size about $100\ \mu\text{m}$. The 'crinkly' line going from the top to the right bottom of the images can be associated with a grain boundary.

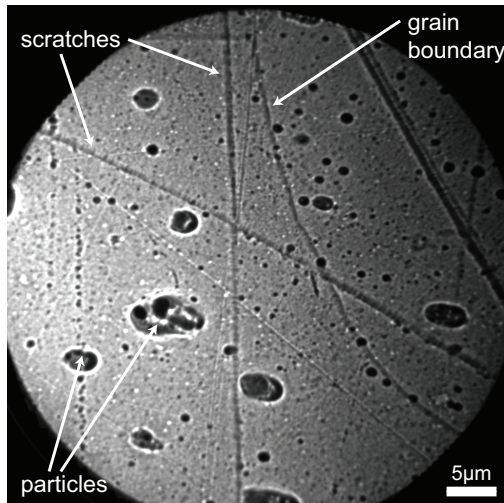


Figure 3.3: MEM image of the pristine aluminium alloy surface.

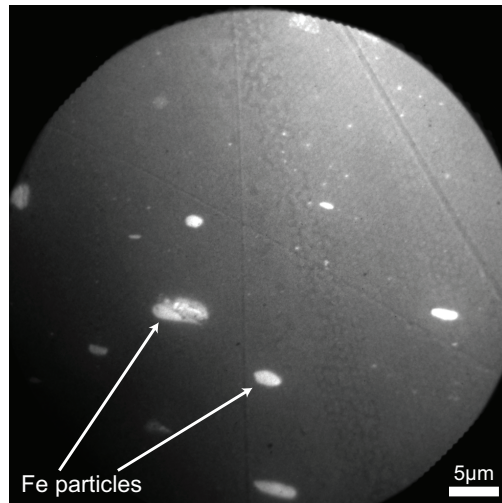


Figure 3.4: XPEEM image for Fe $2p_{3/2}$ taken before heating.

In figure 3.4 an XPEEM image of Fe $2p_{3/2}$ is shown. To be able to reach the Fe $2p_{3/2}$ line, which is at 706.8 eV, the images were acquired in absorption mode. The bright spots in this image correspond to the locations of high iron concentrations. The reason of the scratches appearing in the XPEEM image is that features on the surface add a minor contrast in XPEEM images, as explained previously in section 2.3.3.

Comparing the MEM, figure 3.3, and the XPEEM image, figure 3.4, the oval particles on the surface in the MEM image can be identified as iron particles because their locations coincide with the bright spots in the Fe $2p_{3/2}$ XPEEM image. These images next to each other illustrate how powerful a combination of topographic and chemical information with spatial resolution is. Using the SPELEEM one is able to not only detect features on the surface but determine their chemical composition and electronic state, which makes it a valuable tool for surface science.

3.2.2 XPS and XPEEM

The following XP spectra were obtained from an area of $10 \times 10 \mu\text{m}^2$ of the sample. All XP spectra were normalized with respect to their photoionization cross sections [34], beam current and the photon intensity differences for different photon energies as shown in figure 2.2. All spectra were calibrated to the Fermi level.

Aluminium

Figure 3.5 shows the Al 2p line for three different temperatures, room temperature, 300°C and 400°C, at a photon energy of 120 eV. From the approximate peak position for all three spectra at 76.3 eV, it can be deduced that aluminium oxide and aluminium hydroxide are present at the surface [35]. With increasing temperature the signal corresponding to aluminium oxide is decreasing.

The single peak in the spectrum corresponds to a convolution of a number of different aluminium oxide and hydroxide signals. Different states of aluminium oxide can arise from different chemical environments, meaning e.g. that an aluminium atom at the bulk metal-aluminium oxide film interface is different from an aluminium atom within the oxide film. Another factor contributing to the amount of different signals, which are convoluted into one peak, is that several elements, see table 3.1 are present in the alloy, leading to a series of mixed compounds and hence mixed oxides and hydroxides.

Further, two components from the spin-orbit split are created for each distinct chemical state of aluminium. The width of the peaks of each of the possible components is influenced by experimental factors such as instrumental broadening or the photon energy. Additionally, the natural line width is determined by the lifetime of the excited state. The number of factors that lead to the detected signal illustrate how complex it is to study a system like this.

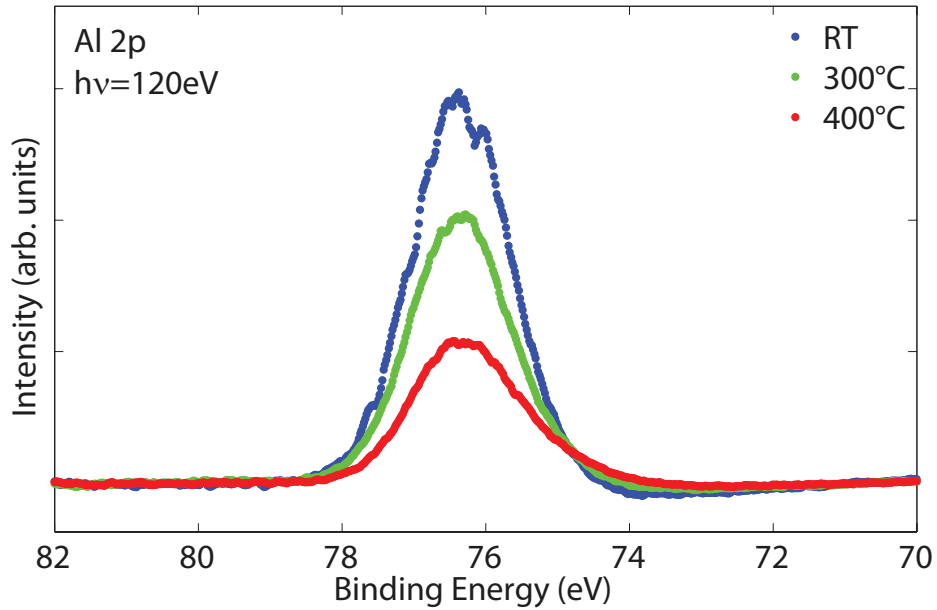


Figure 3.5: XPS spectra of the Al 2p line acquired at $h\nu=120\text{eV}$ for aluminium-magnesium-silicon alloy 6063 at room temperature and after heating to 300°C and 400°C .

Magnesium

In figure 3.6 XPS spectra of Mg 2p at room temperature, 300°C and 400°C are shown. The spectra were collected at a photon energy of 133 eV. The inset in the top right shows the Mg 2p line at 400°C for a photon energy of 133 eV and 180 eV. The approximate peak position for all five spectra is at 52.4 eV, which corresponds to magnesium oxide [35]. It should be noted here again, that the single peak does not stand for pure magnesium oxide but a convolution of several different peaks as explained previously for the aluminium spectra. Comparing the three spectra in the main plot, a clear increase of the magnesium oxide signal with increasing temperature is shown.

By measuring the XPS spectra for the different temperatures at different photon energies, namely 100 eV, 133 eV and 180 eV, depth profiling was performed. Since the attenuation length of the photoelectrons depends on the material through which the electrons have to pass, it is complex to estimate the energy probing-depth relation for a multi component system like an aluminium alloy. Therefore, only qualitative conclusions were drawn from these measurements. However, it was observed that the magnesium signal increases at lower probing depth, i.e. lower photon energy (see figure 3.6). This indicated that magnesium is diffusing towards the surface upon heating. This hypothesis is supported by the XPEEM images for Mg 2p shown in figure 3.7 and figure 3.8.

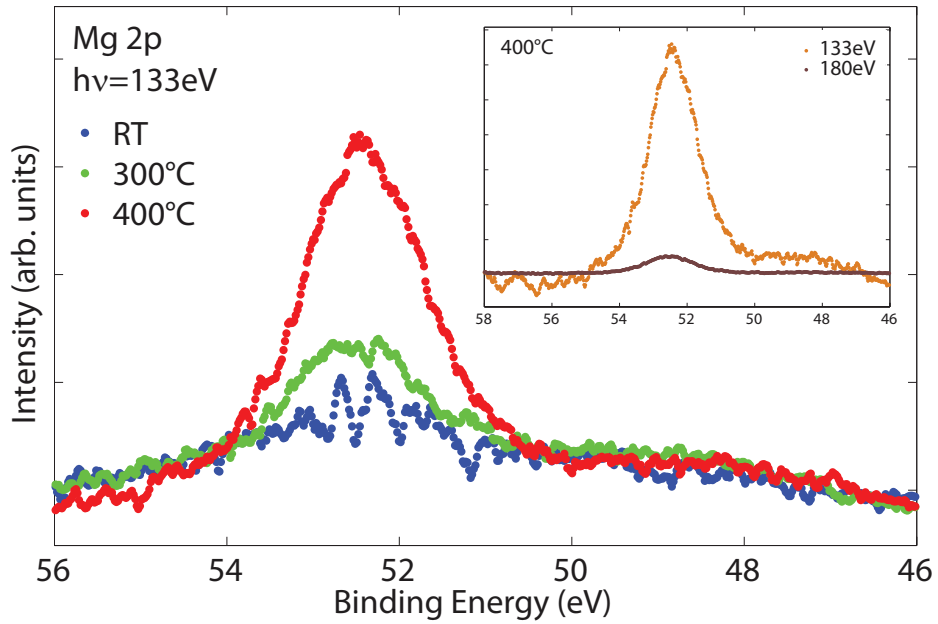


Figure 3.6: XP spectra of the Mg 2p line obtained at $h\nu=133\text{eV}$ for aluminium-magnesium-silicon alloy 6063 at room temperature and after heating to 300°C and 400°C. The inset shows the Mg 2p line at 400°C measured at $h\nu=133\text{eV}$ and $h\nu=180\text{eV}$ as an example for measurements with different probing depth.

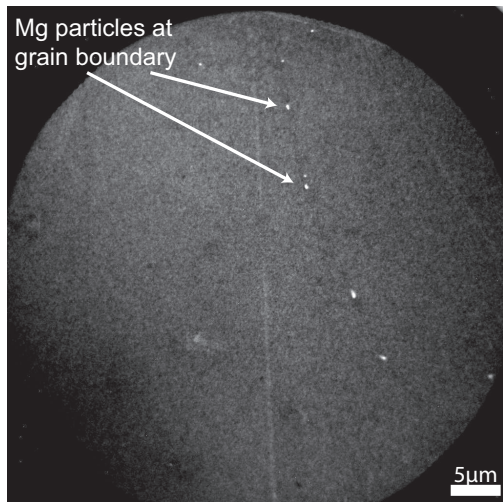


Figure 3.7: XPEEM image for Mg 2p taken after acquisition at 300°C

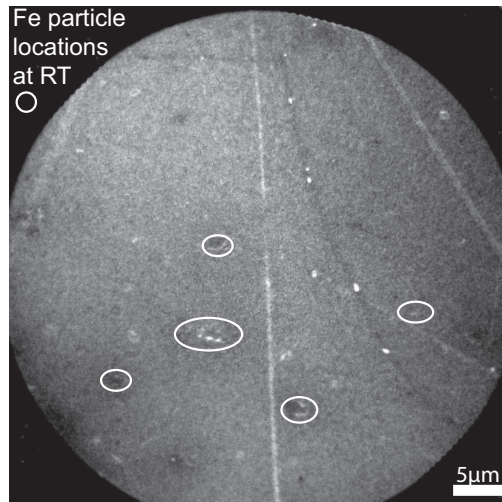


Figure 3.8: XPEEM image for Mg 2p taken after heating to 400°C

Here, the overall brightness of the XPEEM image at 400°C is greater than the one for the XPEEM image at 300°C. A qualitative comparison of brightness is possible due to applying the same greyscale during the processing of the image. This indicates that the overall magnesium content at the surface increased. Further, one can see that magnesium particles are already present at 300°C at the grain boundary going from the top middle of the image to the bottom right.

By comparing the XPEEM image of Mg 2p at 400°C to the XPEEM image of Fe 2p_{3/2} in figure 3.4, one can find that magnesium content increases at locations where iron particles have been before the heating. The approximate locations of some of the iron particles are marked by brown circles in the magnesium XPEEM image.

Silicon

In figure 3.9 the XP spectra for the second major alloying element, silicon, are given. The spectra were collected at a photon energy of 133 eV and show the Si 2p line. The approximate peak position for the room temperature peak is at 104.2 eV and indicates that silicon oxide is present [35]. The approximate peak position of Si at 300°C is slightly shifted towards a lower binding energy of 104 eV. The spectrum measured after heating to 400°C is flatter, wider and shifted further to lower binding energies. This indicates that upon heating silicon oxide is reduced but no elemental silicon is formed. Elemental silicon has a binding energy of about 99 eV [35].

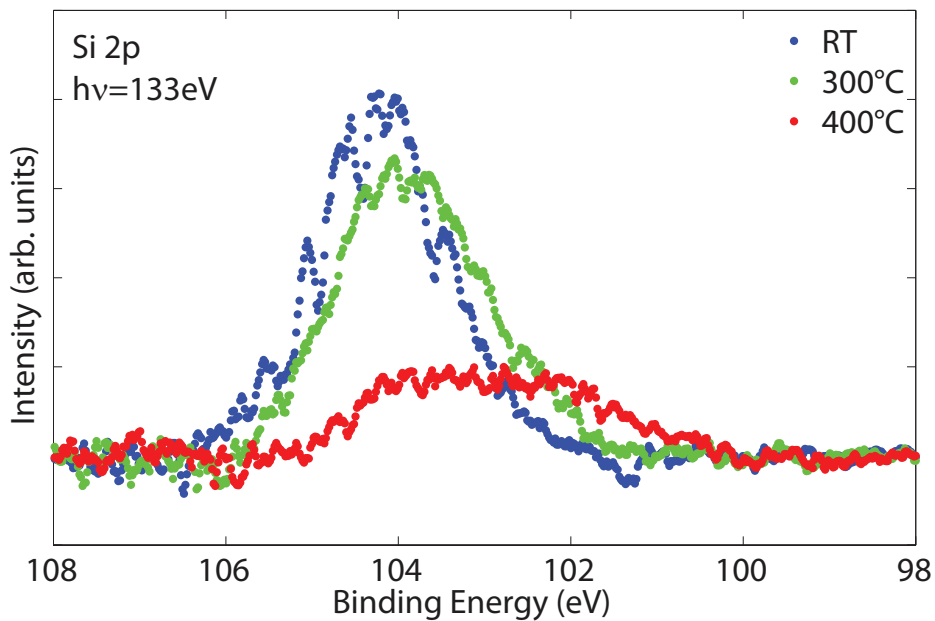


Figure 3.9: XP spectra of the Si 2p line taken at $h\nu=133\text{eV}$ for aluminium-magnesium-silicon alloy 6063 at room temperature and after heating to 300°C and 400°C.

3.2.3 Surface after Heat Treatment

The surface of the aluminium alloy was characterized after the heating by MEM and SEM as shown in figure 3.10 and figure 3.11 respectively. Here, it should be noticed, that the SEM image was taken of the aluminium alloy after exposure to air.

By comparing the MEM image in figure 3.8 and the XPEEM image for magnesium in figure 3.10, one can see that the bright spots in the XPEEM image of magnesium occur at the same locations as surface particles are indicated by the MEM image. This together with the increased intensity in the Mg 2p spectrum at 400°C, shown in figure 3.6, gives strong indication that the particles segregating at the surface are composed of magnesium mainly.

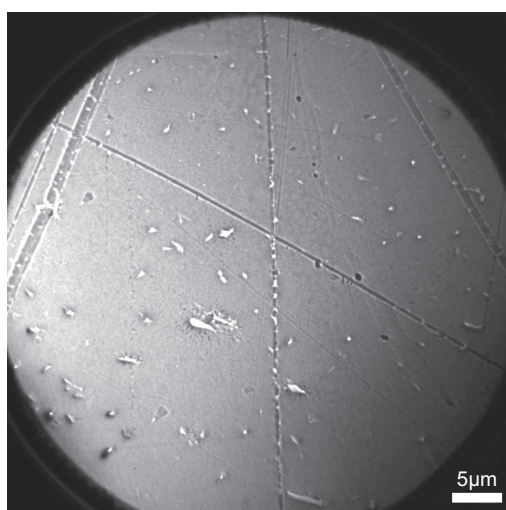


Figure 3.10: MEM image taken after heating to 400°C.

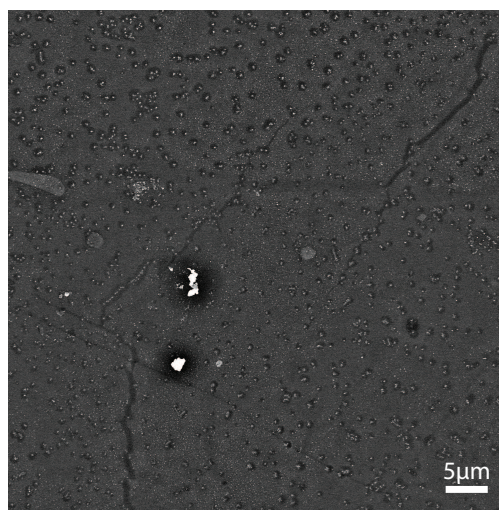


Figure 3.11: SEM image of taken after heating to 400°C and exposure to air.

3.2.4 Summary

The pristine aluminium-magnesium-silicon alloy 6063 consists of base aluminium alloy covered by a native aluminium oxide film. Additional to the aluminium oxide, magnesium oxide and silicon oxide were detected in the surface layer by using XPS, see figures 3.5 till 3.9. On the surface distinct iron particle were identified using a combination of MEM and XPEEM images for Fe 2p_{3/2}, see figure 3.3 and 3.4.

Upon heating to 400°C the magnesium content was found to increase in surface layer and magnesium particles segregated at the surface, as indicated by the XP spectra for the Mg 2p line, figure 3.6, and the XPEEM images for Mg 2p, figures 3.7 and 3.8. Already in the magnesium XPEEM image at 300°C, magnesium particles can be found at the grain boundary. Silicon oxide is reduced by heating the sample to 400°C but no elemental silicon is formed, see figure 3.9.

3 Aluminum-Magnesium-Silicon Alloy 6063

The formation of mixed oxides, aluminides and silicides is a possible explanation for this. Through depth dependent spectra it was found that silicon is diffusing into the base alloy.

An illustrative summary of the processes just described is shown in figure 3.12. There it should be noted, that the chemical formulas are representative for a possible range of different compounds forming among the aluminium and its alloying elements.

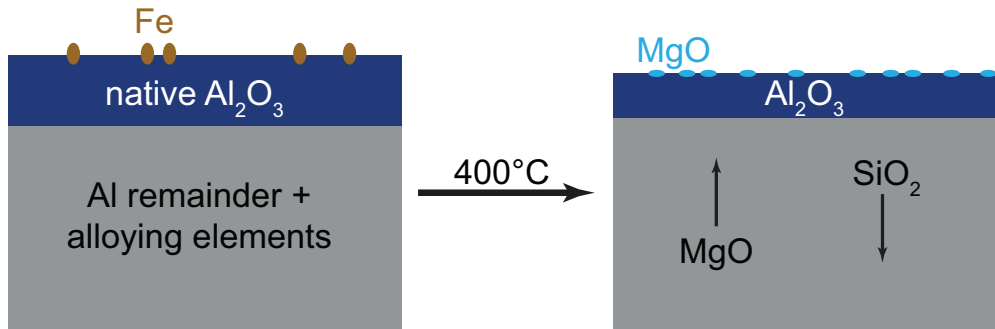


Figure 3.12: Simplified graphic summarizing the processes taking place during heat treatment of the aluminium-magnesium-silicon alloy 6063.

4 Industrial Alloy for Brazing Applications

Joining aluminium pieces together can be done in different way, e.g. welding, mechanical joining and brazing. The alloy described in this section is designed for brazing applications. During brazing a liquid phase of the brazing alloy, also called braze cladding, is formed upon heating. The liquid alloy is then drawn between the different close-matched work pieces by capillary forces. Even though the brazing alloy is supposed to melt, the core material should remain solid. By cooling the braze cladding the different workpieces are joined together. After brazing hardening of the alloy is still possible. An advantage of joining workpieces through brazing is that different metals can be joined while containing a high thermal conductivity as required in e.g. heat exchangers.

The aluminium alloy sample that was studied here is illustrated in figure 4.1. It consists of a core material, also referred to as base alloy, and a braze cladding. The base aluminium alloy is alloyed with manganese, copper, magnesium, iron silicon and titanium. Each of the alloying elements amounts for less than 1 wt%. The brazing alloy is an aluminium-silicon alloy with a silicon content of 7.5-12 wt%. Other minor alloying elements are magnesium, iron and bismuth. The braze cladding accounts for approximately 12% of the outermost layer on each side of the workpiece. Here, that gives a thickness of the brazing alloy of about $50\mu\text{m}$. The braze cladding is covered by a native aluminium oxide film, which needs to be broken up to allow proper brazing. Brazing of this specific alloy takes place in HV (10^{-5} torr) at approximately 600°C . This is just high enough to melt the braze cladding, which has a melting point of about 580°C , but low enough to leave the base alloy, which has a melting point above 615°C , intact.

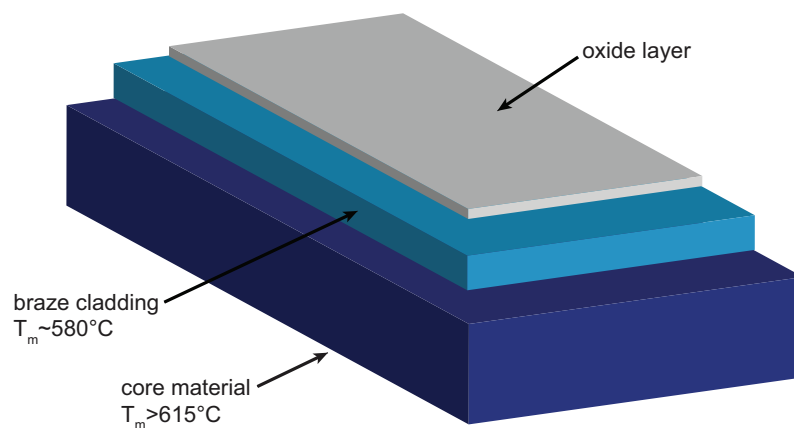


Figure 4.1: Image illustrating the composition of an aluminium alloy designed for brazing applications. (Not drawn in scale.)

It is important to know at which temperature the aluminium oxide layer breaks up and how the surface changes during melting of the braze cladding because it influences the wetting, ability of the liquid phase to stay in contact with the solid phase, and the capillary effects. Only surfaces with high wetting can be strongly joined together because then no major defects are created in the brazing alloy after cooling.

4.1 Experimental Procedure

The experimental procedure for this sample is very similar to the one described for the aluminium-magnesium-silicon alloy 6063 in chapter 3.1. Only the temperatures to which the alloy was heated before the spectra were acquired at the SPELEEM changed.

The experiments were performed in two sessions. During the first session measurements were performed after subsequent heating to 400°C and 500°C. Apparently, the sample started to melt at 500°C already, so no measurements at higher temperatures could be carried out due to problems with discharging. In the second session a new sample was used and smaller temperature steps were chosen. Data was acquired at 380°C, 420°C, 460°C and 480°C. The sample was heated further to 490°C but partial melting occurred, so measurements were not possible any more.

As for the aluminium-magnesium-silicon alloy 6063 SEM images were taken ex-situ before and after the heating in the SPELEEM for both samples. Additionally, images with an optical microscope were obtained for the sample of the first session after melting its surface.

4.2 Results

4.2.1 Pristine Surface

In figure 4.2 the SEM image of the pristine surface is shown. Several particles with an diameter in the range of 1µm to 7µm have been identified for both samples.

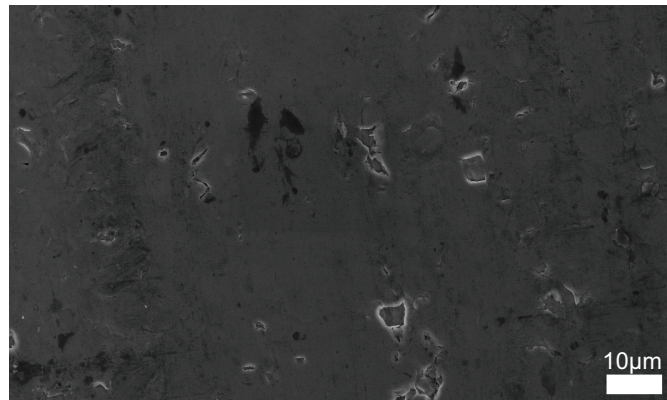


Figure 4.2: SEM image of the pristine surface of the aluminium-silicon alloy used as braze cladding in industrial alloys.

4.2.2 XPS and XPEEM

As for the previously presented data, the XP spectra were all normalized with respect to their photoionization cross sections [34], beam current and the photon intensity differences for different photon energies as shown in figure 2.2. All spectra were calibrated to the Fermi level.

Aluminium

In figure 4.3 the combined data of both sessions for the Al 2p line is shown. The spectra were obtained at a photon energy of 133 eV. The spectrum at 380°C has an approximate peak position of 76.3 eV, which corresponds to aluminium oxide and hydroxide [35]. By heating the sample from 380°C to 400°C the aluminium oxide signal increases. Heating further to 420°C the intensity decreases again and at 460°C the intensity decreased further and the peak shifts 0.4 eV towards lower binding energies. At 480°C the peak has shifted to 73.1 eV, which corresponds to metallic aluminium [35]. Through heating to 500°C a steep increase in the intensity for the metallic peak occurs.

The binding energy shift at 460°C indicates that mixed aluminium compound starts to occur at this temperature, either through diffusion or reduction of aluminium oxide. The disappearance of the aluminium oxide peak and the appearance of a metallic aluminium peak at 480°C indicated that the aluminium oxide layer is almost completely removed and aluminium is present at the surface layer.

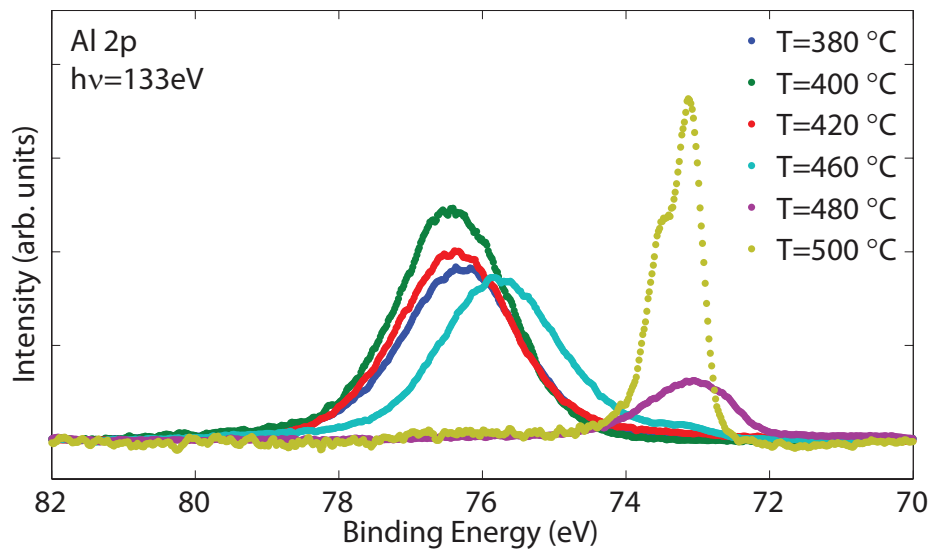


Figure 4.3: XP spectra of the Al 2p line acquired at $h\nu=133$ eV after heating aluminium alloy to 380°C, 400°C, 420°C, 460°C, 480°C and 500°C subsequently.

The occurrence of metallic aluminium at a temperature of 480°C and above is supported by the SEM and optical microscope images in figures 4.9 to 4.13. There, a partial melting

of the surface at 490°C is shown. At 500°C the surface melted completely and only small islands of aluminium oxide are preserved at the surface, see 4.13.

Magnesium

In figure 4.4 the combined XP spectra of the Mg 2p line of the first and the second experimental sessions are shown. The spectra were acquired at a photon energy of 133 eV. The spectra obtained between 380°C and 460°C have peak positions in the region of magnesium oxide [35]. After heating to 480°C a strong signal for metallic magnesium occurs and the signal for magnesium oxide nearly disappears. By heating the sample to 500°C no major peak in the Mg 2p line could be detected. The sudden occurrence of the metallic magnesium peak can be understood by considering the diffusivity of magnesium in aluminium increases rapidly at elevated temperatures. The segregation of magnesium at the surface at 480°C was detected in the XPEEM image for Mg 2p, see figure 4.6, too.

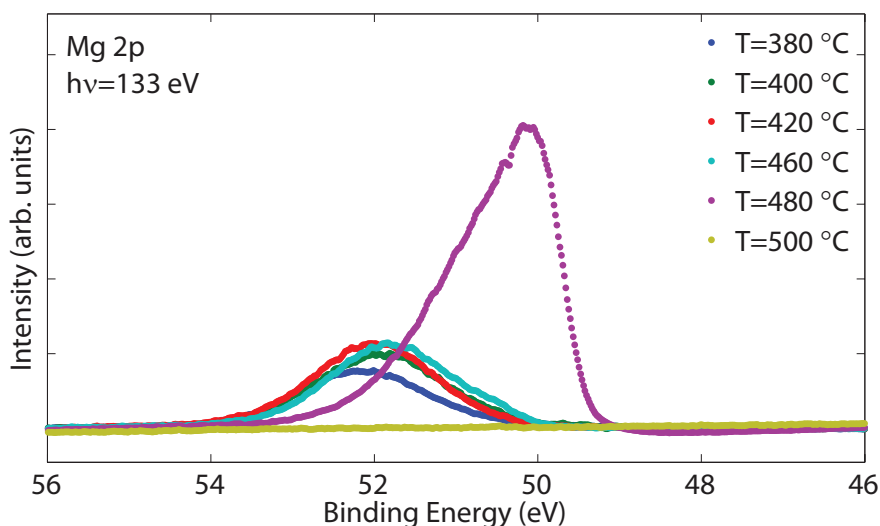


Figure 4.4: XP spectra of the Mg 2p line obtained at $h\nu=133$ eV after heating aluminium alloy to 380°C, 400°C, 420°C, 460°C, 480°C and 500°C subsequently.

In figures 4.5 and 4.6 XPEEM images for Mg 2p at 380°C and 480°C are shown. The contrast in figures 4.5 is strongly enhanced and gives rather topographic information than chemical. Hence, the magnesium content at the surface layer at 380°C is minor. To remove the contrast due to the surface topography in figure 4.6, an XPEEM image was acquired slightly off-peak and then subtracted from the XPEEM image at the Mg 2p peak, to create the shown image. Here, particles with a high magnesium content can be identified. The diameter of these particles ranges approximately from 0.2 μm to 1.7 μm . The segregation of magnesium particles to the surface at 480°C is in accordance with the strong increase in the metallic magnesium signal in the XP spectrum in figure 4.4.

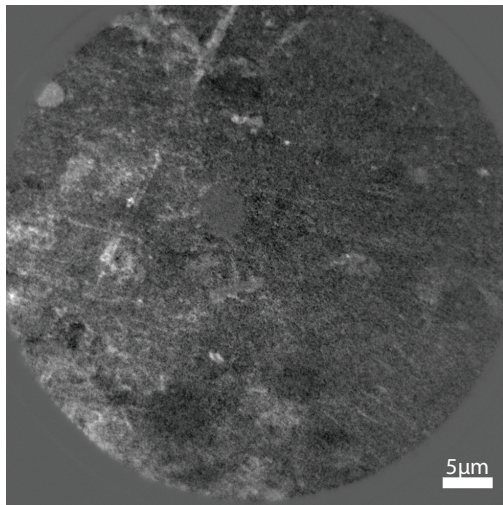


Figure 4.5: XPEEM image for Mg 2p taken after heating to 380°C.

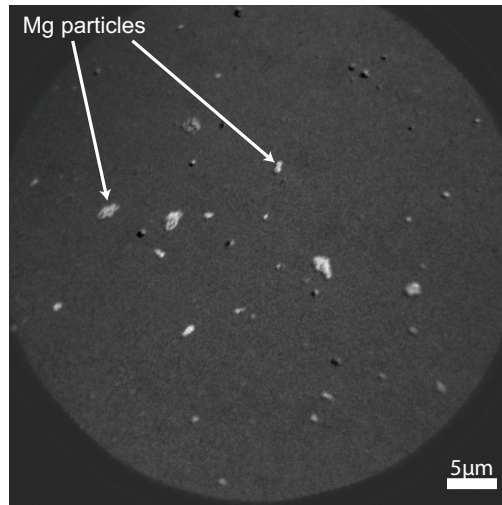


Figure 4.6: XPEEM image for Mg 2p taken after heating to 480°C.

Silicon

Figure 4.7 shows the XP spectra from the second session for Si 2p obtained at a photon energy of 133 eV. The peak position indicated that silicon oxide is present in the surface layer [35]. A slight increase in intensity occurs by heating to 420°C. The intensity of the silicon oxide signal decreases by heating to 460°C and shifts slightly to lower binding energies. At 480°C no significant amount of silicon could be detected.

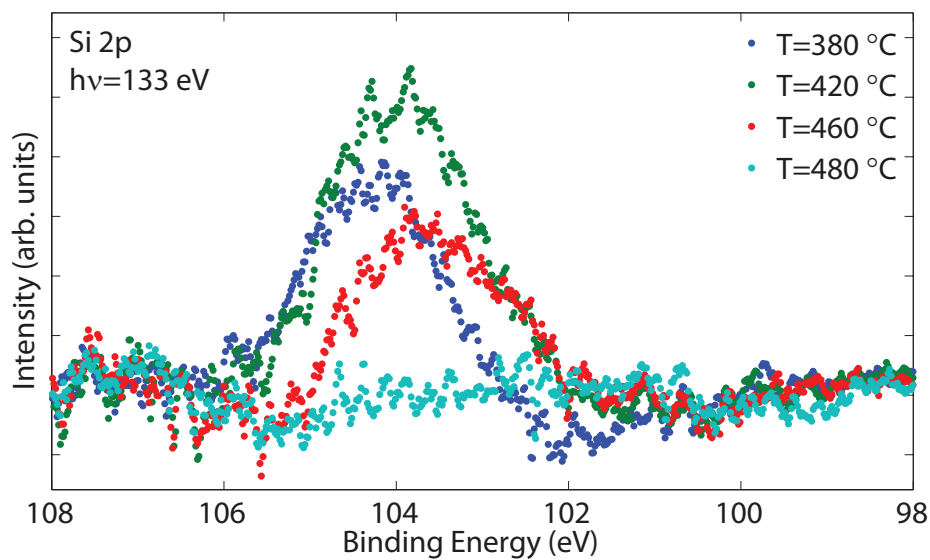


Figure 4.7: XP spectra of the Si 2p line obtained at $h\nu=133$ eV after heating aluminium alloy to 380°C, 400°C, 420°C, 460°C, 480°C and 500°C subsequently.

The signal intensity of the silicon XP spectra is significantly lower than that for magnesium. This indicates that even though the absolute concentration of silicon in the braze cladding is higher than the one of magnesium, less silicon is present in the surface layer.

Oxygen

During the second experiment oxygen spectra were obtained, too. In figure 4.8 XP spectra for the O 1s line are plotted. The data were acquired at a photon energy of 580 eV. The broad peak that was detected here, is in the binding energy region which is expected to correspond to a convoluted signal of aluminium oxide and aluminium hydroxide [35]. A similar trend as for the silicon spectra is observed for the oxygen spectra. By heating to 420°C the intensity of the signal increases and by heating to 460°C it decreases again. At 480°C no major oxygen signal was detected.

The disappearing of the oxygen signal at 480°C agrees well with the changes in the XP spectra for aluminium, magnesium and silicon, figures 4.3, 4.4 and 4.7 respectively. In these spectra the corresponding oxide signals disappeared at 480°C, too. This is an indication for the sudden sublimation of a metal oxide. Here, it should be noted, that a pressure increase in the vacuum chamber of the SPELEEM occurred around that temperature.

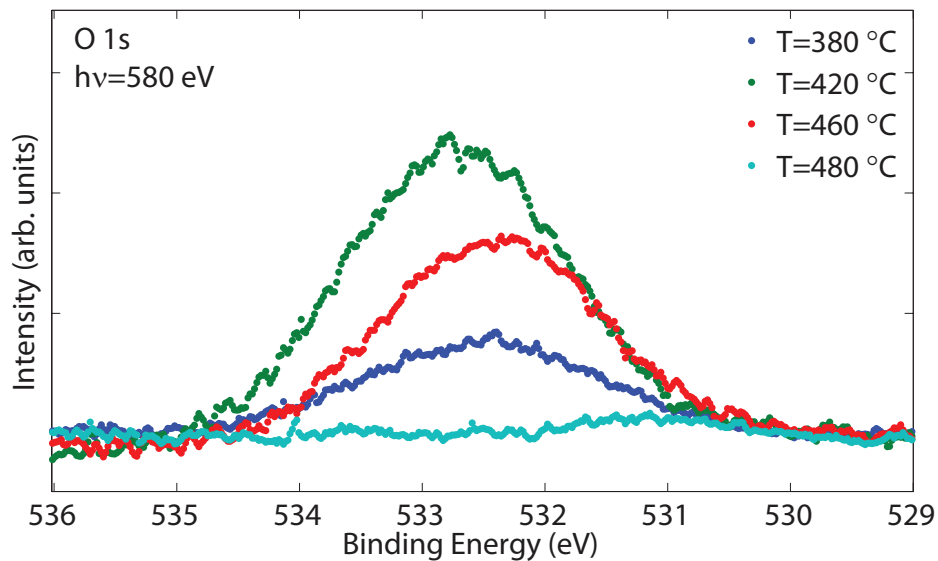


Figure 4.8: XP spectra of the O 1s line obtained at $h\nu=580$ eV after heating aluminium alloy to 380°C, 400°C, 420°C, 460°C, 480°C and 500°C subsequently.

4.2.3 Surface after Heat Treatment

Since the experiment was performed in two sessions, two different sample surfaces are shown here. In the second session the sample was only heated up to 490°C. Therefore, figures 4.9 and 4.10 show SEM images with different scales taken ex-situ after the heating within the SPELEEM. In figure 4.9 small holes in the surfaces indicate that the partial melting occurred by heating to 490°C. In figure 4.10 particles with a similar size as the previously identified magnesium particles in XPEEM, see figure 4.6, were found at the surface.

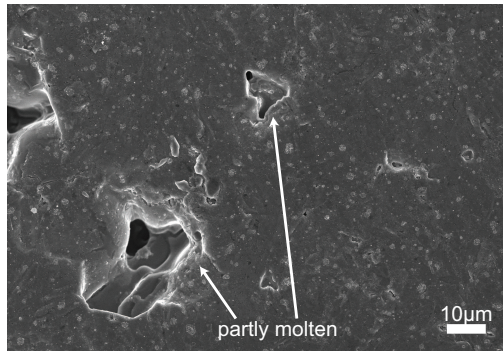


Figure 4.9: SEM image after heating to 490°C

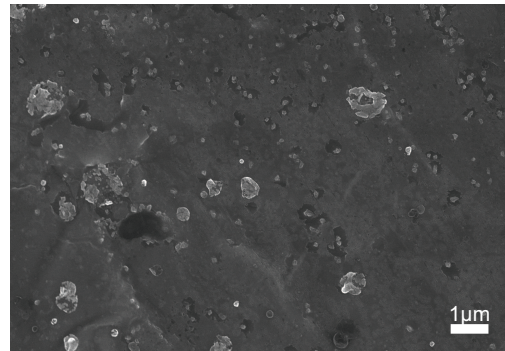


Figure 4.10: SEM image after heating to 490°C.

The sample of the first session was heated to 500°C. In figure 4.11 a images acquired by an optical microscope directly after dismantling the sample. It shows that the sample surface was completely molten after heating to 500°C.

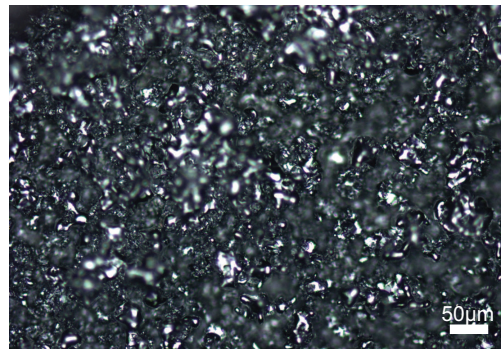


Figure 4.11: Image obtained by an optical microscope.

However, by taking a closer look with a SEM small areas can be identified, where the oxide layer was preserved, see figure 4.13. These oxide islands seem like they have been floating on the melted surfaces as shown in figure 4.12.

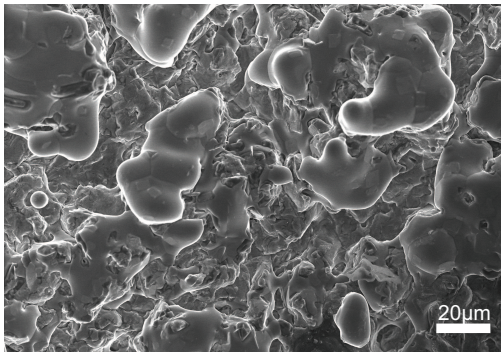


Figure 4.12: SEM after heating to 500°C.

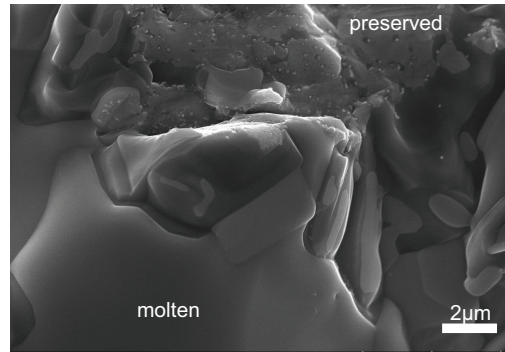


Figure 4.13: SEM after heating to 500°C.

4.2.4 Summary

Throughout the heat treatment of the aluminium alloy in UHV, we were able to follow the decomposition of the oxide layer covering the braze cladding. It was observed that at 480°C the XP signals for oxygen, aluminium oxide, magnesium oxide and silicon oxide disappear. Further, signals corresponding to metallic aluminium and magnesium occur. Using XPEEM the segregation of magnesium-rich particles at the surface was observed at 480°C. At 490°C partial melting of the surface layer was discovered. Subsequent heating of the sample to 500°C lead to the disappearance of the metallic magnesium peak in the XP spectrum and a further increase in intensity of the metallic aluminium signal. It was found that the surface layer was molten at 500°C but small areas of the oxide layer were preserved. The islands were identified using SEM. Unfortunately, no MEM and XPEEM images of the sample surface could be obtained at temperatures above 480°C because of problems with discharging due to the high surface roughness.

5 Comparison and Discussion

The results of the heat treatment of two different aluminium alloy samples were presented. Both samples were studied with the SPELEEM during the heating cycles and characterized ex-situ with SEM before and after the experiment. The main difference between the samples is their composition. In the aluminium alloy 6063 the main alloying element is magnesium with 0.45-0.9 wt.% and only 0.2-0.6 wt.% silicon are added. The main alloying element in the brazing alloy is silicon with a much higher concentration about 9.7 wt.%. The magnesium content in the braze cladding is less than 1 wt.%, which is similar to the one in the aluminium alloy 6063. However, each of the samples forms a native oxide layer on the surface upon exposure to an oxidizing environment like air.

Generally, for both samples peaks in the XP spectra were rather wide. This indicates that a variety of signals is represented by a single peak consisting of a convolution of the single species. For the aluminium oxide peaks this means that actually besides aluminium oxide, aluminium hydroxide, and mixed aluminium oxides containing one or several of the alloying elements, e.g. spinel, are present. Possibly the local formation of magnesium aluminides like Mg_2Al_3 and $\text{Mg}_{17}\text{Al}_{12}$ need to be considered [36], too. In the case of magnesium and silicon magnesium silicide can form. Magnesium silicide is known to contribute to the strengthening in aluminium based alloys [3,32]. Additional to the different chemical components, different peaks for bulk and surface components can be included in the peaks, too. Thus, wide peaks are hardly avoidable when conducting experiments on alloys and their oxides.

For both samples a decrease in aluminium oxide intensity upon heating was observed, see figures 3.5 and 4.3. This might be partially due to the fact that magnesium oxide is thermodynamically favoured over aluminium oxide and hence, the diffusion of magnesium towards the surface could lead to a reduction of aluminium [37]. Another possibility is that aluminium oxide sublimates due to the low pressure and elevated temperature. The occurrence of a metallic aluminium signal for the brazing alloy can be explained by the melting of the surface layer at temperatures of 480°C and above.

In XP spectra and XPEEM images of both samples the diffusion and segregation of magnesium at the surface was observed, see figures 3.6, 3.8, 4.4 and 4.6. The diffusion of magnesium to the surface can be understood by considering the high diffusivity of magnesium in aluminium [38]. Also, it explains the increase in magnesium signal upon heating. Further, it is interesting, that magnesium particles are present at the grain boundary after heating to 300°C only as shown in 3.7. This shows that grain boundary diffusion of magnesium takes place lower temperatures before the bulk diffusion occurs [39]. The disappearance of the magnesium oxide signal at 480°C for the brazing alloy can be explained by the sublimation of magnesium oxide. The presence of metallic magnesium in the braze cladding has the same reason as the metallic aluminium signal:

5 Comparison and Discussion

the surface layer starts melting at 480°C. At 500°C no metallic magnesium was detected. The silicon XP spectra of both samples indicate that silicon oxide is present at first, see figures 3.9 and 4.7. For the aluminium-magnesium-silicon alloy 6063 a decrease in the intensity of the signal and a shift to lower binding energies was detected. This indicates that silicon is reduced but no signal corresponding to elemental silicon was obtained. However, for the braze cladding an increased intensity for the silicon oxide peak by heating to 420°C was noticed. Through subsequently heating to 460°C a decrease was observed. At 480°C no major silicon signal was acquired.

XP spectra for oxygen were only obtained for the brazing alloy. In figure 4.8 the oxygen peak first increases by heating to 420°C. This might be due to the diffusion of dissolved oxygen towards the surface. The decrease of the oxygen peak and its disappearance at 480°C goes together with the disappearing of the aluminium oxide and magnesium oxide signals at 480°C. This can be associated with the sublimation of the oxides as described previously.

Even though the compositions of the two studied samples are different, similar trends were observed during the heat treatment experiments.

The processes, which took place during the heat treatment in the alloy, can not be transferred one to one to what is happening during the manufacturing or brazing of the studied alloys because the experiments presented here were performed in UHV. During the manufacturing aluminium alloys are far way from experiencing these low pressures and even during brazing they are only exposed to HV. However, the here presented experiments can show trends in the behaviour of the studied aluminium alloys during heat treatment.

6 Conclusion and Outlook

The work presented in this thesis is an example of how powerful the combination of MEM, XPEEM, XPS and SEM is to study alloy surfaces. For both aluminium alloys it was possible to determine the elements present at the surface layer and their chemical state. Further, XPEEM in combination with MEM gave the opportunity to locate artefacts on the surface and determine their composition. This combination allows to obtain element specific information with spatial resolution, too. Therefore, it was possible to observe that grain boundary diffusion of magnesium takes place at 300°C before the bulk diffusion.

The here presented study of the aluminium-magnesium-silicon alloy 6063 shows how elevated temperatures affect the distribution and chemical state of the alloying elements and the composition of the oxide layer. This information can be used to reconsider the processing of the alloy. Especially during ageing, the alloy is exposed for a long time to increased temperatures, which might also lead under atmospheric pressure to a diffusion of magnesium towards the surface. Non-uniformly distributed magnesium might lead to a weakening of the material. Therefore, one needs to compromise the gain in strength by growing coherent precipitates during ageing and the loss due to non-uniformly distributed alloying elements.

For the alloy designed for brazing applications it was found that at 480°C the oxides sublimate and metallic aluminium and magnesium are present at the surface. By using the SEM images small island of preserved oxide were identified. Melting the braze cladding but having oxide particles still present can lead to inclusions, which later might cause an earlier failure of the join.

Problematic for studying alloys is that multiple mixed compounds of all the elements are possibly present in the sample. Since many of them are chemically very similar they are hard to distinguish by the used techniques. However, the differences between oxidized, reduced and metallic species could be identified. Possibilities to illuminate, which compounds can be expected to exist in the sample under certain conditions, are given by range of thermodynamic and kinetic calculations. These might be a useful asset to further studies.

Another problem that occurred during the measurements is the determination of the correct temperature of the sample in the vacuum chamber of the SPELEEM. The here used thermocouple gives only a reading for the temperature close to the sample but not of the sample itself because it is only attached to the sample holder. Additional measurements with a pyrometer are not correct either because emissivity of the surface is changing during the heating. Finding a reliable solution to obtain the sample temperature will be important for future experiments.

6 Conclusion and Outlook

Further, the resolution of the XP spectra obtained with the SPELEEM is not optimal. To fit several components to one peak might be difficult even if calculation are available predicting which phases and compounds to expect. Therefore, high resolution XPS measurements using the spectroscopy endstation at beamline I311 were performed but not yet analysed. Measurements at higher pressures are planned, too. By using the HP-XPS (High Pressure X-ray Photoelectron Spectroscopy), measurements under more realistic conditions will be possible.

From HE-XPS (High Energy X-ray Photoelectron Spectroscopy) measurements at the ESRF (European Synchrotron Radiation Facility) that are not presented here, it seems as if most minor alloying elements can only be detected when using hard x-rays. This is an indication for the minor alloying elements being present further in the bulk and not at the upper surface layer. Further experiments using HE-XPS are planned to study how the minor alloying elements are effected by heat treatment.

7 Self-reflection

While analysing the data and writing this thesis, I got a more and more complete picture of what we actually measured during the experiments and more importantly, what that means. By putting it all together, I also noticed what I would have liked to add, what we did not measure, and what we should have done differently.

One example is that we only took XPEEM images for iron for the aluminium-magnesium-silicon alloy 6063 at room temperature but not after the heating. This was partly due to time restriction during the beamtime but also because at that point, we did not know that the iron particle might become really interesting. However, we did see, after analysis, that magnesium seems to segregate at the surface, where we detected iron particles at room temperature.

Another example is that the alloy used in brazing applications melted already at 500°C. We were somewhat surprised that it melted about 80°C lower in UHV than the expected melting point at atmospheric pressure. Clearly, the temperature measurements during the experiment need to be improved. However, the initial idea was to heat to 400°C, then to 500°C and then in smaller steps up to the melting point. So we repeated the experiment and started with smaller temperature steps at 380°C.

Generally, I would have been nice to look into the minor alloying elements, too. Even though the magnesium content in both alloys is less 1 wt.% the intensities detected were higher after normalizing with respect to their different cross sections than for silicon, which amounted for nearly 10 wt.% in the brazing alloy. Thus, some of the minor alloying elements might actually play an important role.

Besides the planning of experiments and discovering how the samples react, I learned a lot about how to handle raw data. Importing, adjusting grey scales, creating spectra out of images, subtracting backgrounds, analysing, and eventually creating a somewhat presentable figure, took me some time to figure it all out but after I sorted all the data and had all the MATLAB scripts ready and done the routines several times, it became fun.

Especially while writing the thesis I improved my latex skills and found some nice tricks. By now creating figures with illustrator does not take that long anymore, either.

Finally, I learned that I really like to study alloys. They are kind of messy systems but that makes the challenge. Now easy and straight forward solution that are given at the end of the textbook but playing around with a range of concepts and coming up with some strange ideas is actually entertaining. Believe it or not!

In the end, I believe that the topic is not the most important thing though. If you have nice supervisors and an enthusiastic and open working atmosphere, you can become excited about anything. Therefore, I would like to thank everybody how was involved in this project again. It was a pleasure to work with all of you! Thanks!

Bibliography

- [1] W. Miller, L. Zhuang, J. Bottema, A. Wittebrood, P. D. Smet, A. Haszler and A. Vieregge. “Recent development in aluminium alloys for the automotive industry”. *Materials Science and Engineering: A*, 280(1), 37–49, 2000. doi:10.1016/S0921-5093(99)00653-X.
- [2] P. Peck. *Interest in Material Cycle Closure? Exploring Evolution of Industry’s Responses to High-grade Recycling from an Industrial Ecology Perspective*. Ph.D. thesis, Lund University, 2003.
- [3] W. Martienssen and H. Warlimont. *Springer Handbook of Condensed Matter and Materials Data*. Berlin, Heidelberg: Springer-Verlag, 2005. doi:10.1007/3-540-30437-1.
- [4] R. Lumley. *Fundamentals of aluminium metallurgy : production, processing and applications*. Cambridge : Woodhead Publishing Limited, 2010. doi:10.1533/9780857090256.
- [5] M. Busse, A. Herrmann, K. Kayvantash and D. Lehmkus. *Structural Materials and Processes in Transportation*. Hoboken: Wiley, 2013. doi:10.1002/9783527649846.
- [6] R. E. Hummel. *Understanding Materials Science: History · Properties · Applications*. New York: Springer-Verlag, 2005. doi:10.1007/b137957.
- [7] M. Easton and D. H. St. John. “Improved prediction of the grain size of aluminum alloys that includes the effect of cooling rate”. *Materials Science and Engineering: A*, 486, 8–13, 2008. doi:10.1016/j.msea.2007.11.009.
- [8] R. K. Bolingbroke, A. Gray and D. Lauzon. “Optimisation of Nocolok™ Brazing Conditions for Higher Strength Brazing Sheet”. SAE Technical Paper 971861, 1997. doi:10.4271/971861.
- [9] J. Zähr, S. Oswald, M. TÜRpe, H. Ullrich and U. Füssel. “Characterisation of oxide and hydroxide layers on technical aluminum materials using XPS”. *Vacuum*, 86(9), 1216–1219, 2012. doi:10.1016/j.vacuum.2011.04.004.
- [10] J. W. Diggle, T. C. Downie and C. W. Goulding. “Anodic oxide films on aluminum”. *Chemical Reviews*, 69(3), 365–405, 1969. doi:10.1021/cr60259a005.
- [11] J. D. Jackson. *Classical electrodynamics*. New York : Wiley, 1999.

Bibliography

- [12] A. Liénard. “Champ Électrique et Magnétique”. *L'Éclairage Électrique*, 16, 5–14, 53–59, 106–112, 1898.
- [13] A. Hofmann. *The Physics of Synchrotron Radiation*. Cambridge University Press, 2004.
- [14] K. Wille. *The physics of particle accelerators : an introduction*. Oxford : Oxford University Press, 2000.
- [15] R. Nyholm, J. Andersen, U. Johansson, B. Jensen and I. Lindau. *Nuclear Instruments and Methods in Physics Research Section A: Accelerators, Spectrometers, Detectors and Associated Equipment*, 467 - 468, Part 1, 520 - 524, 2001. doi:10.1016/S0168-9002(01)00399-0.
- [16] “<http://www.elmitec-gmbh.com/>”. Web, 19 Mar 2014. ELMITEC Elektronenmikroskopie GmbH.
- [17] S. Hüfner. *Photoelectron spectroscopy : principles and applications*. Advanced texts in physics. Berlin : Springer, 2003. doi:10.1007/978-3-662-09280-4.
- [18] V. Schmidt. “Photoionization of atoms using synchrotron radiation”. *Reports on Progress in Physics*, 55(9), 1483–1659, 1992. doi:10.1088/0034-4885/55/9/003.
- [19] H. Hertz. “Über einen Einfluss des ultravioletten Lichtes auf die elektrische Entladung”. *Annalen der Physik*, 267(8), 983–1000, 1887. doi:10.1002/andp.18872670827.
- [20] A. Einstein. “Über einen die Erzeugung und Verwandlung des Lichtes betreffenden heuristischen Gesichtspunkt”. *Annalen der Physik*, 322(6), 132–148, 1905. doi:10.1002/andp.19053220607.
- [21] “http://www.nobelprize.org/nobel_prizes/physics/laureates/1921/”. Web, 13 Feb 2014. The Nobel Prize in Physics 1921, Nobel Media AB.
- [22] K. Siegbahn. “Electron Spectroscopy for Atoms, Molecules, and Condensed Matter”. *Science*, 217(4555), 111–121, 1982. doi:10.1126/science.217.4555.111.
- [23] “http://www.nobelprize.org/nobel_prizes/physics/laureates/1981/”. Web, 13 Feb 2014. The Nobel Prize in Physics 1981, Nobel Media AB.
- [24] C. Schneider. *Soft X-ray photoelectron emission-microscopy (X-PEEM)*. Springer Netherlands, 2006. doi:10.1007/1-4020-3337-0_8.
- [25] J. Feng and A. Scholl. *Photoemission Electron Microscopy (PEEM)*. New York: Springer, 2007. doi:10.1007/978-0-387-49762-4_9.
- [26] J. Stohr and S. Anders. “X-ray spectro-microscopy of complex materials and surfaces”. *IBM Journal of Research and Development*, 44(4), 535–551, 2000. doi:10.1147/rd.444.0535.

Bibliography

- [27] E. Bauer. “A brief history of PEEM”. *Journal of Electron Spectroscopy and Related Phenomena*, 185(10), 314–322, 2012. doi:10.1016/j.elspec.2012.08.001.
- [28] W. Świech, B. Rausenberger, W. Engel, A. Bradshaw and E. Zeitler. “In-situ studies of heterogeneous reactions using mirror electron microscopy”. *Surface Science*, 294(3), 297–307, 1993. doi:10.1016/0039-6028(93)90116-2.
- [29] G. F. Rempfer and O. H. Griffith. “Emission microscopy and related techniques: Resolution in photoelectron microscopy, low energy electron microscopy and mirror electron microscopy”. *Ultramicroscopy*, 47, 35–54, 1992. doi:10.1016/0304-3991(92)90184-L.
- [30] R. F. Egerton. *Physical Principles of Electron Microscopy: An Introduction to TEM, SEM, and AEM*. Boston, MA : Springer Science+Business Media, Inc., 2005. doi:10.1007/b136495.
- [31] “<http://www.aluminum.org/resources/industry-standards>”. Web, 2 May 2014. Industry Standards, The Aluminium Association.
- [32] J. R. Davis (Editor). *Metals handbook. Vol. 2, Properties and selection: nonferrous alloys and pure metals*. American Society for Metals International, 1990.
- [33] Chakrabarti and D. E. Laughlin. “Phase relations and precipitation in Al-Mg-Si alloys with Cu additions”. *Progress in Materials Science*, 49, 389–410, 2004. doi:10.1016/S0079-6425(03)00031-8.
- [34] J. Yeh and I. Lindau. “Atomic subshell photoionization cross sections and asymmetry parameters: $1 \leq Z \leq 103$ ”. *Atomic Data and Nuclear Data Tables*, 32(1), 1–155, 1985. doi:10.1016/0092-640X(85)90016-6.
- [35] C. Wagner, W. Riggs, L. Davis, J. Moulder and G. Muilenberg. *Handbook of X-ray Photoelectron Spectroscopy*. Perkin-Elmer Corporation, Physical Electronics Division, Minnesota, U.S.A., 1979.
- [36] D. Singh, C. Suryanarayana, L. Mertus and R.-H. Chen. “Extended homogeneity range of intermetallic phases in mechanically alloyed Mg-Al alloys”. *Intermetallics*, 11(4), 373–376, 2003. doi:10.1016/S0966-9795(03)00005-0.
- [37] C. V. Robino. “Representation of mixed reactive gases on free energy (Ellingham-Richardson) diagrams”. *Metallurgical and Materials Transactions B*, 27(1), 65–69, 1996. doi:10.1007/BF02915078.
- [38] K. N. Kulkarni and A. A. Luo. “Interdiffusion and Phase Growth Kinetics in Magnesium-Aluminum Binary System”. *Journal of Phase Equilibria and Diffusion*, 34(2), 104–115, 2013. doi:10.1007/s11669-013-0189-2.
- [39] H. Mehrer. “Diffusion: Introduction and Case Studies in Metals and Binary Alloys”. In P. Heitjans and J. Kärger (Editors), “Diffusion in Condensed Matter”, Springer Berlin Heidelberg, 2005. doi:10.1007/3-540-30970-5.1.